Coexistence of impurity-induced quasi-one-dimensional electronic structure and topological surface states of Bi_2Se_3

R. Shokri[a)]
Max-Planck-Institut für Mikrostrukturphysik, Weinberg 2, D-06120 Halle, Germany

(Received 1 December 2015; accepted 5 February 2016; published online 23 February 2016)

Using scanning tunneling spectroscopy (microscopy) (STS, STM) in combination with angle-resolved photoelectron spectroscopy (ARPES), we report on the coexistence of the topological surface state with a long range periodic modulation of the electronic structure on the surface of Bi_2Se_3 at room temperature. The electronic modulation manifests itself as a two-dimensional commensurate superlattice characterized by stripes running parallel to the surface lattice vectors when the near-surface region of samples are doped with trace amounts of iron or cesium. In both cases, the electronic signature is observed in STM only at energies within the valence band more than 130 meV blow the Dirac point energy (E_D). ARPES experiments show the presence of intact Dirac cone, indicating that the electronic stripes do not influence the Dirac surface states. We suggest that the stripe states are the bulk properties of Bi_2Se_3 induced by trace amounts of cesium and iron impurities residing in bismuth and selenium substitutional sites and/or in the van-der-Waals gap. [http://dx.doi.org/10.1063/1.4942220]

I. INTRODUCTION

Ordered electronic modulations imposed on the periodic potential landscape of surfaces are of great importance in several systems. For example, stripe- or checkerboard-like charge ordering have been one of the main challenges in understanding high temperature superconductivity in cuprates,[1,2] or similarly in doped graphene sheets, quasi one-dimensional electronic modulations might be related to the emergence of superconductivity.[3] In some layered materials like transition metal chalcogenides, ordered electronic states give rise to nonlinear transport properties.[4–6] Thus, it is crucial to disentangle the rich variety of electronic states of matter that may coexist and to figure out whether the coexisting phases are independent or interacting with one another. In this context, STM as a real-space local probe is a powerful technique to discern between multiple interacting periodicities.[1,7–11]

While for several low-dimensional materials, electronic superlattices have been extensively studied, for bismuth chalcogenides, there are just a few studies in this direction due to lack of experimental observations.[12–16] The layered compound Bi_2Se_3 and its cousin Bi_2Te_3 belong to the family of three dimensional topological insulators (3D TIs), an unusual type of matter as they are insulators in the bulk but metals at the surface.[17–20] The fundamental property of TIs is that the topological surface state (TSS) is robust against perturbations such as structural defects, vacancies, dislocations, and adsorbed impurity species as long as time reversal symmetry (TRS) is preserved.

Owing to its large band gap of 0.3 eV, Bi_2Se_3 is viewed as an archetype material, and a great wealth of attempts have been made to manipulate its structural and electronic properties.[21–27] For instance, the near-surface structure of a single crystal or an ultrathin film of Bi_2Se_3 has been precisely examined using surface x-ray analysis[26] or a possibility of tuning its surface band structure related to surface structural modification through doping the near surface region has been illustrated.[27] It has been shown that the surface of Bi_2Se_3 is not chemically inert, which may have interesting applications.[28–30] To this end, by exposing the surface of Bi_2Se_3 to atomic hydrogen, a long-range ordered bismuth-bilayer-terminated Bi_2Se_3(1000) is synthesized,[28] or by Fe deposition followed by annealing, epitaxial FeSe nanocrystals on Bi_2Se_3 are prepared.[29]

In this work, we provide evidence that trace amounts of two different doping species (iron and cesium) located in the near (0001) surface region of the topological insulator Bi_2Se_3 leads to the formation of new long range ordered periodic electronic states, which are observed as stripe-like patterns in STM images. STM topographic images and conductance maps reveal a periodic surface potential landscape commensurate with the two dimensional surface of the host lattice, which only exists at energies below $U = E_D$–130 meV, where E_D is the Dirac energy. Simultaneously, ARPES experiments clearly show the presence of the TSS, indicating the coexistence of the TSS and the stripe electronic ordering. We propound that the electronic stripes do not influence the surface states and are related to the bulk properties of Bi_2Se_3. Our results might provide new strategies for engineering the electronic and thermoelectric properties of topological insulators in general.

II. METHODS

The experiments were carried out in an ultra-high-vacuum chamber (base pressure of 1×10^{-10} mbar) equipped with an Auger electron spectrometer, low energy electron diffraction (LEED), and an Omicron variable temperature STM. Bi_2Se_3 single crystals (with a rhombohedral crystal structure and space group R–3 m) were cleaned by Ar^+ sputtering at 0.5–2 keV followed by annealing at 400–500 °C. Surface

[a)]Electronic mail: roozbeh.shokri80@gmail.com

cleanliness and long range order was verified by STM, Auger electron spectroscopy (AES), and LEED. Surface preparation leads to atomically flat terraces with lateral extensions of several hundred nanometers.[26,27] The sample preparation was carried out in three steps. In the first step, about 50% of a monolayer (ML) of iron or cesium were deposited on the pristine surface kept at room temperature (RT), keeping the pressure in the range of 10^{-10} mbar during deposition.[31] Here, and in the following, we refer to 1 ML as being equivalent to 6.74×10^{14} atoms/cm^2, i.e., one adatom per substrate atoms. AES spectra clearly indicated the presence of iron (LMM) and cesium (MNN) Auger transitions, respectively.[31] In the second step, the as-deposited samples were annealed at 170 °C for several minutes leading to an in-diffusion of the adsorbents into the bulk.[31] Previous studies[30,32] have shown the high tendency of iron to diffuse into the Bi_2Se_3 bulk at elevated temperatures, thereby substituting bismuth atoms. Also, cesium atoms—when deposited at RT—strongly interact with the Bi_2Se_3(0001) surface by initially replacing top layer selenium atoms,[33] similar to what is observed for dosing the surface with atomic hydrogen.[28] In the third step, the samples were treated by prolonged Ar^+ sputtering in the range between 20 min and 5 h followed by another annealing step at 400–500 °C. This procedure removes about 4 to 50 quintuple layers (QL), leading to an apparently clean and flat surface as examined by AES,[31] STM, and LEED, the latter reflecting the $p3m1$ plane group symmetry as the pristine sample. Throughout the entire paper, the annealing temperatures for the demonstrated results are 170 °C in the second step and 450 °C in the third step, otherwise it is mentioned. Following this three step preparation procedure, STM experiments were carried out at RT. In this investigation, we focus on STM imaging carried out at RT, while the STS spectra were collected at 25 K ($V_{mod} = 8$ mV, $f_{mod} = 4$ kHz).

Momentum resolved photoemission experiments were carried out using a momentum microscope.[34] The doped Bi_2Se_3 samples were illuminated by p-polarized 6 eV photons radiation from the 4th harmonic of a Ti:Sapphire laser (pulse-length 300 fs with a repetition rate of 80 MHz), under an angle of incidence of 22° with respect to the sample surface, along the M-Γ-M direction (along the horizontal k_x axis in Figures 3(A) and 3(B)). Photoelectrons emitted into the complete solid angle above the sample surface (emission angles of ±90° are detected) were collected by the objective lens of a photoelectron emission microscope. Without the need of mechanical sample movement like in conventional ARPES measurements, the image of the photoemission intensities as a function of the lateral crystal momentum (k_x, k_y) is obtained in the focal plane of the objective lens. Series of constant energy momentum images in steps of 10 meV, energy filtered using an aberration compensated electrostatic analyzer, were recorded by a CCD camera from a fluorescent screen image detector. The experimental data, consisting of about 70 of these (k_x, k_y) momentum distribution images along the binding energy axis, allows us to select the band dispersion E($k_{||}$) along arbitrary directions in the surface Brillouin zone (SBZ). This is displayed for the $\bar{K} - \bar{\Gamma}$ and $\bar{\Gamma} - \bar{M}$ directions. We note that, by the momentum microscope measurement principle, it is straight forward to choose E($k_{||}$) such that the section runs precisely through the Dirac point at the SBZ center, avoiding the ambiguity of conventional ARPES measurements where a gap-opening might be wrongly observed due to sample misalignment. Here, we do not observe a gap for either the Fe-doped or the Cs-doped samples.

III. RESULTS

A. Quasi-1D electronic modulation characterized by STM and STS

Topographic STM images in Figures 1(A)–1(F) illustrate for the iron and cesium doped samples the observed stripe patterns and their bias voltage dependence. The strong energy dependence of the patterns clearly indicates their electronic origin. If the bias voltage is chosen corresponding to tunneling out of occupied states within the bulk band gap, in both cases the hexagonal arrangement of bright dots is observed, which is attributed to surface selenium atoms (A and D). In addition, several triangular defects are visible which are commonly attributed to defects such as subsurface bismuth vacancies, anti-site defects, and selenium defects (see A and D).

Dirac points were determined through STS (see Figure 2). If the bias voltage (U) is increased to probe states below the D_p (below $U = E_D$–130 meV and $U = E_D$–200 meV for iron and cesium, respectively), a dramatic change in the topographic images is observed (see Figures 1(B) and 1(E)). Schematic of the band structure is outlined in Figure 1(G). In both cases, periodic stripe patterns appear, which are commensurate with the Bi_2Se_3 two dimensional surface lattice (will be discussed later in the text). Figure 1(H) demonstrates the LEED pattern of the iron-doped (or similarly for Cs-doped) sample. The LEED pattern corresponds to Bi_2Se_3, excluding any possible surface reconstruction or adatom ordering. Here, we note that the stripe structures cover almost 100% and approximately 70% of the surface area in the case of the iron and cesium doped sample, respectively.

B. ARPES experiments and the electronic band structure

ARPES experiments were performed to investigate the electronic structures of Fe and Cs-doped Bi_2Se_3. Figure 3 illustrates the electronic band structure of Fe and Cs-doped Bi_2Se_3 after 30 min sputtering followed by annealing. The band structure was found to remain unchanged within the temperature range from 120 K to RT. The ARPES clearly confirms that the time reversal symmetry protection of TSS is not lifted and the Dirac point remains intact. Both spectra confirm the presence of the TSS with an intact D_p located at ca. 280 meV (Fe) and 330 meV (Cs) below the Fermi-level. Prolonged Ar^+ sputtering results in a shift of the Dirac Energy towards the Fermi-level, but does not retain exactly the same value as the pristine surface. The position of the D_p below $U = E_F$ corresponds to n-doping of the sample, which is attributed to the presence of selenium defects. Interestingly, the energy position of the D_p in the case of the cesium doped sample located about 50 meV below that of the iron doped sample. This is tentatively attributed to an increased density of selenium defects, most likely induced by cesium atoms, which tend to substitute selenium atoms

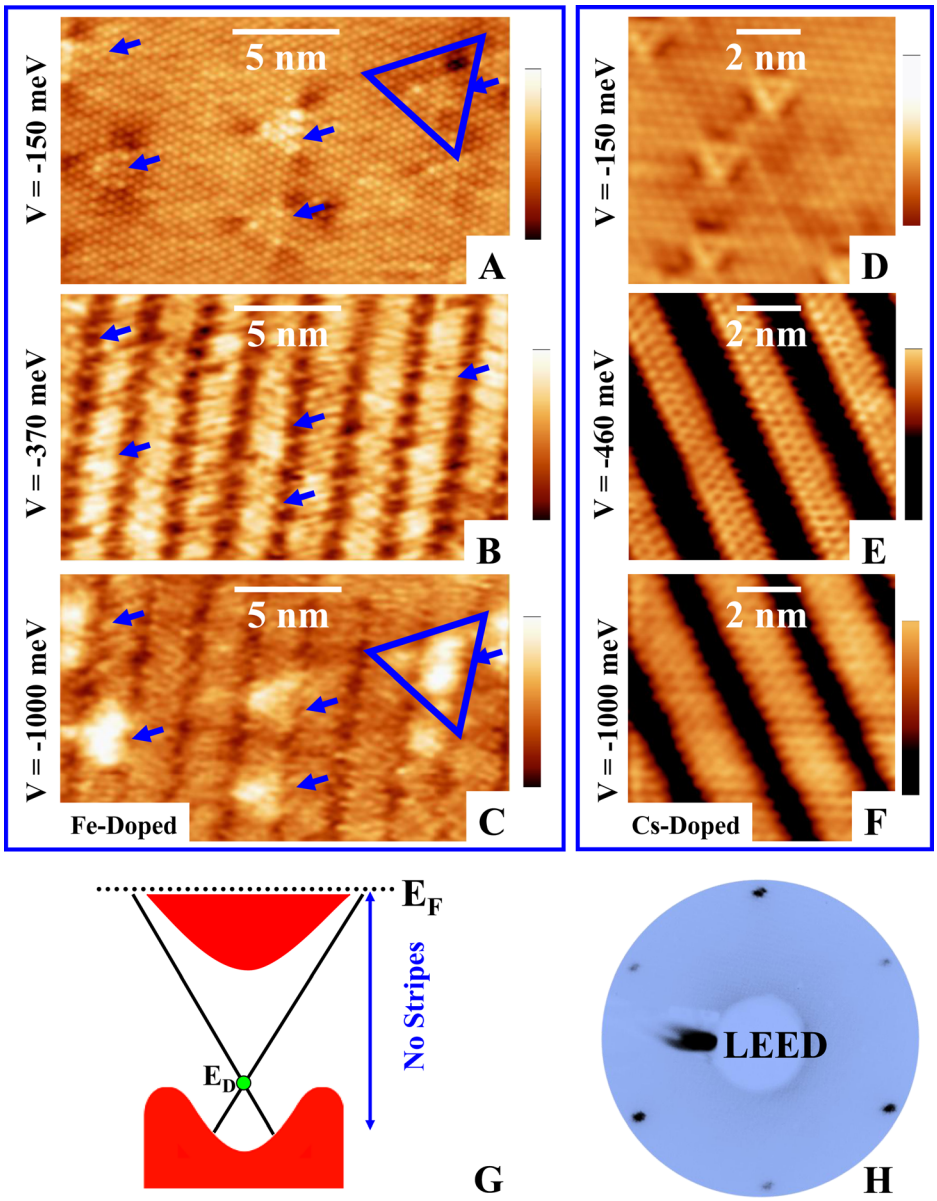

FIG. 1. Bias voltage dependence of the stripe states. STM images are shown for Fe-doped in (A)–(C) and for Cs-doped in (D)–(F) after 5 h sputtering followed by annealing. (G) Schematic representation of the stripes' energy dependence. The arrows in (A)–(C) indicate the identical surface defects. One of the defects is highlighted by the blue triangle in (A) and (C). (H) is a typical LEED pattern of samples containing the stripe phase reflecting the *p3m*1 plane group symmetry as the pristine sample. I = 1000 pA for (A)–(C) and (D), I = 50 pA for (E) and (F). The color scale bar is 0–1.4 Å for (A)–(C) and 0–2.5 Å for (D)–(F).

when deposited in low amounts on the $Bi_2Se_3(0001)$ surface. The defects observed in Figure 1(A) were found in pristine, Fe- and Cs-doped $Bi_2Se_3(0001)$ surface, and their contrast in the STM images can be changed by tuning the tunneling current and/or bias voltage. We did not observe any of the Fe defects reported previously,[37] indicating that the surface is atomically clean. In contrast, the defects discerned in Figure 1(D) are exclusive to Cs-doped samples implying that they are created by Cs atoms. The density of the defects shown in Figure 1(D) was calculated to be ca. 4×10^{-4} Å^{-2} almost twice the defects observed in Figure 1(A). The stronger downward shift of the Dirac point for Cs-doped sample can be understood by taking into account the higher density of Cs defects and regarding that Cs has one electron in the outer shell (electron donor). The similar trend has been previously reported for Cs-doped $Bi_2Se_3(0001)$.[23]

C. Differential conductance map on the stripes

To get a deeper insight into the electronic structure of the surface, the spatial variations of the local density of states (LDOS) was measured. Figure 4(B) exhibits the typical conductance map of the Fe-doped sample. Periodic order of low and high stripe-like LDOS implies that a periodic potential landscape on the (0001) plane (attributed to the bulk states) coexists with TSS. The stripe periods do not change with bias, thus ruling out the dispersing effects such as standing waves and Friedel oscillations. The stripe states recognized in the conductance map down to almost 1.5 eV below the Dirac point. At such low energies, the band structure of Bi_2Se_3 consists of bulk continuum states and does not have a well-defined surface state.[38] For Cs-doped samples, since the stripes could be imaged just at low tunneling currents (lower than 50 pA), due to low signal to noise ratio, no conductance maps could be obtained.

D. Detailed analysis of the electronic superstructure

We now focus on the electronic superstructure. The stripes are about 2 nm in width and have a complicated internal structure. While for the iron doped samples, the stripes are characterized by a zig-zag arrangement of bright wires, for the cesium doped samples, they are characterized by a

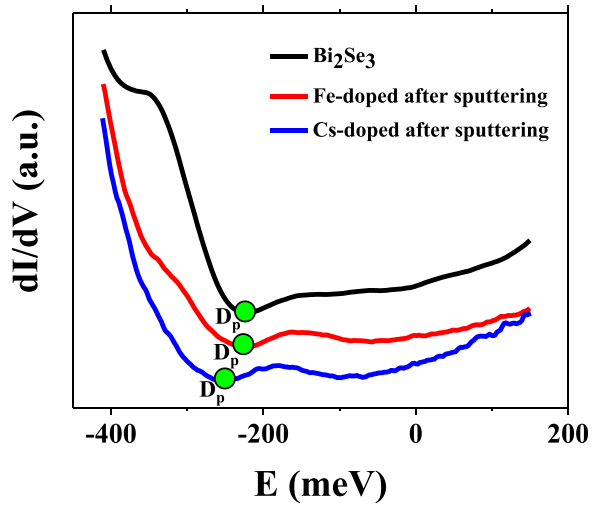

FIG. 2. Averaged dI/dV spectra of the bare Bi_2Se_3, Fe, and Cs-doped samples, measured on the normal Bi_2Se_3 phase far from the surface defects or impurities, after 5 h sputtering followed by annealing. The minima of the differential conductance (attributed to the Dirac points[35,36]) curves was found to be at −225 meV for bare, at −235 meV for Fe-doped, and at −260 meV for Cs-doped surfaces. For doped samples for shorter sputtering time the Dirac point shifts more downward. The set points of STS are 200 pA and 100 meV for Bi_2Se_3, 350 pA and 150 meV for Fe-doped, and 200 pA and 130 meV for Cs-doped.

quasi-hexagonal dot-like internal structure with a higher apparent corrugation of the whole pattern as compared to the iron doped samples. Direct comparison of the images which were taken at the same positions of the sample shows that the stripes are aligned parallel to the hexagonal lattice vectors of the Bi_2Se_3 substrate. Stripes attributed to CDWs with a comparable periodicity have been previously observed by transmission electron microscopy in the bulk of the bulk-doped Bi_2Se_3[12–14] nanowires.

A more detailed analysis of the stripe patterns is outlined in Figure 4, where STM constant current images (A, E) and their Fourier Transforms (FT) (C, F) are discussed. The stripe patterns related to iron and cesium doped samples are of different shape and periodicity. Figures 4(C) and 4(F) show the FTs of large STM topographic images (not shown). The origin of the reciprocal lattice is labeled by (0, 0) and the yellow arrow, while the yellow dashed circles represent the spots related to the Bi_2Se_3(0001) substrate surface. The densely spaced blue spots in Figures 4(C) and 4(F) are related to the stripe patterns, which allow the detailed analysis of the electronic stripe superstructure metric. For the iron doped sample, we find that the matrix (M) relating the real space unit cells of the stripe superlattice to the Bi_2Se_3 surface unit cell is given by: $M_{Fe} = (a_{11} = 3;\ a_{12} = 0;\ a_{21} = 0;\ a_{22} = 12)$. The corresponding unit cell parameters are $a_0 = 12.42$ Å, $b_0 = 49.68$ Å, and $\gamma = 60°$. For the cesium doped sample, we obtained $M_{Cs} = (a_{11} = 1;\ a_{12} = 0;\ a_{21} = 0;$ and $a_{22} = 7)$ with $a_0 = 4.14$ Å, $b_0 = 28{,}98$ Å, and $\gamma = 60°$. In Figures 4(A) and 4(E), the corresponding cells are represented as white parallelograms. Finally, Figures 4(C) and 4(F) show profiles along the reciprocal direction of the stripe lattices, indicating peaks at positions corresponding to the twelve- and sevenfold periodicity of the patterns with respect to the Bi_2Se_3 lattice (see Figures 4(D) and 4(G)).

E. Stripes and sample preparation

In the Method section, we explained that the sample preparation was carried out in three steps, i.e., first, depositing Fe or Cs on the surface; second, annealing the sample at 170 °C; and third, sputtering the surface followed by annealing at 450 °C. Here, we have focused on the measurements performed after the third step, where the electronic superstructure spans hundreds of nanometers. Indeed, the third step of the sample preparation is of central importance for preparing an atomically clean surface with a simple stoichiometric Bi_2Se_3 surface structure as reflected in the STM and LEED data in Figures 1(A), 1(D), and 1(H), as well as AES spectra demonstrated in the supplementary material.[31] Thus, we avoided directing the experiments towards studying a complicated surface structure obtained after the second step of sample preparation.[31,32] Upon annealing in the second step, because of the in-diffusion of the adsorbents, many new defects are created, and accordingly, the surface is very rough and covered partially with adatoms or islands of atoms.[31,32] However, we point out that the electronic superstructure was already observed after the second step. Therefore, the role of sputtering in the third step should not be considered as a related factor to emergence of the stripe phase. We argue that several hours of sputtering (the test experiments were performed up to 10 h at 1 KeV) did not lead to vanishing the stripe phase, indicating that the embedded impurities in the near-surface region cannot be completely removed by sputtering. However, we found that by mechanical cleavage of Bi_2Se_3 in vacuum using an adhesive tape, the stripe phase finally disappeared. We were able to identify the electronic superstructure for 3 out of 3 samples for Cs-doped and for 2 out of 3 samples for Fe-doped.

IV. DISCUSSION

Finally, we comment on the possible origin of the electronic modulation. The stripe phase cannot be attributed to CDWs originated from the backscattering between the TSS. We note that the energy range in which the stripe phase was revealed (far from E_D) is consistent with the fundamental property of topological insulators, i.e., the backscattering between spin-polarized $\mathbf{k}$ and $-\mathbf{k}$ states on the opposite sides of the Fermi contour is forbidden; thus, the pairing required for CDW transition is prohibited for the TSS. ARPES measurements (Figures 3(A) and 3(B)) reveal just a small Dirac cone deformation (hexagonal warping), which may not provide resilience to backscattering for the formation of CDWs.[39,40] Moreover, the analysis of FTs in Figure 4 (see Figures 4(C) and 4(F)) gives rise to $q_{stripe-Fe} = 0.13$ Å^{-1} and $q_{stripe-Cs} = 0.2$ Å^{-1}, which unambiguously demonstrate that the values of $\mathbf{q}$ cannot be ascribed to the scattering between the surface states near to the Dirac node, where the maximal radius of the Dirac cone is less than 0.1 Å^{-1}. Therefore, the electronic band structure shown in Figure 3 cannot support the Fermi surface (FS) nesting and the formation of CDWs related to TSS. In addition, for the sputtered samples, we do not observe the formation of 2DEG or Rashba-split states, which can be prone to CDW instabilities.[41,42]

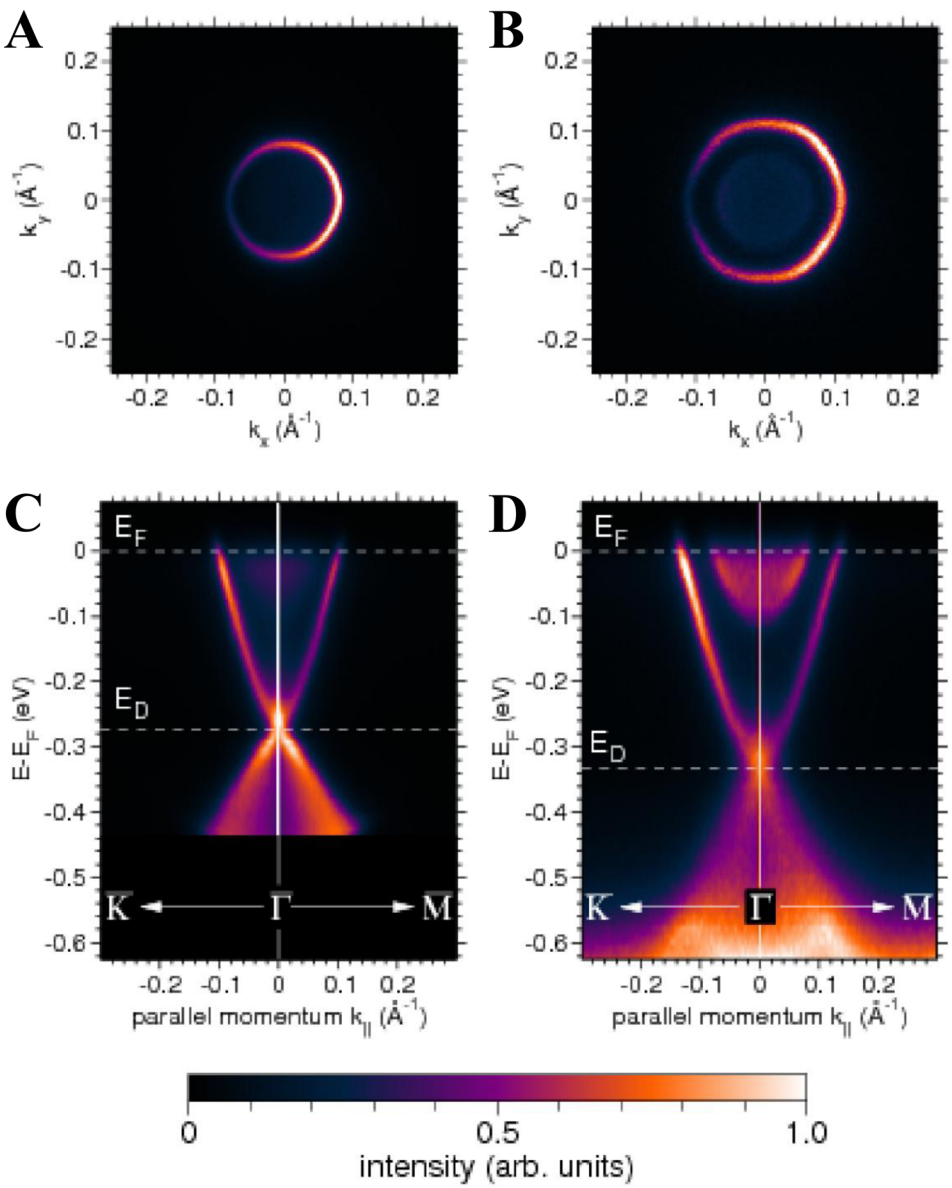

FIG. 3. Electronic band structure of Fe and Cs-doped Bi_2Se_3 after sputtering and annealing measured by ARPES at a temperature of 120 K. (A) and (C) Fe-doped and (B) and (D) Cs-doped. The FS maps are shown in (A) and (B). (C) and (D) are the band dispersions along the $\bar{K}-\bar{\Gamma}$ and $\bar{\Gamma}-\bar{M}$ directions.

The similar stripe phase attributed to CDWs with a comparable periodicity has been recognized as the bulk properties of cobalt or indium/cobalt doped Bi_2Se_3.[12–14] However, it should be noted that CDW should be observed by STM below and above the Fermi level with opposite contrast in the STM topographic images, while we do not see the stripes above the Fermi level.

In analogy to the phenomena observed in this work, oscillating behavior induced by charged defects has been noticed on the (110) surface of n-doped III-V semiconductors, only at occupied states.[43] We suggest that the Fe or Cs impurity (or defect) plays a similar role as the charged defects. The appearance of the stripe patterns is interpreted as being an electronic structure induced by impurities buried in the bulk of Bi_2Se_3. Embedded impurity atoms induce a local variation of the band bending at the surface, which in turn involves a depletion or accumulation of electrons in the valence band close to the surface depending on whether the tip probes unoccupied or occupied states, respectively.[44] Owing to the large screening length in semiconductors the local change of the LDOS as a result of the electron density variation is imaged by the STM, even if the impurity atoms reside several nanometers below the surface.[44] Accordingly, the stripe patterns are observed only by probing valence band states but disappear when the STM probes the TSS, which is primarily located within the top QL. Moreover, we argue that albeit the stripes are observed at the surface, regarding the energy range in which they are observed and considering that TSS remains intact (except the shift of the Dirac point), they are most likely not related to the surface state but rather are the bulk state properties.

In parallel with this observation, the LEED pattern in Figure 1(G) does not show any trace of surface reconstruction since LEED probes the top few atomic layers of the first QL at most. In consequence, these results suggest that the stripe patterns resemble the periodic electronic lattice of the bulk Bi_2Se_3 crystal, doped by iron and cesium. To better understanding of the origin of the stripes, further investigation can be done by determining the precise atomic position of Fe and Cs atoms and calculating the band structure of

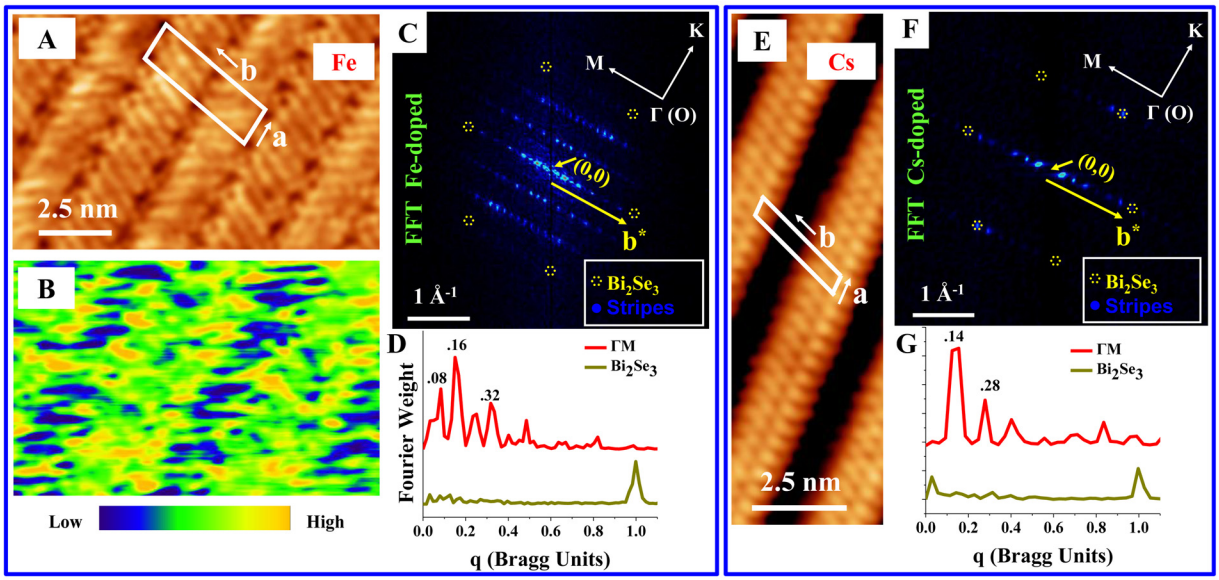

FIG. 4. Analysis of the stripes lattices. (A)–(D) Fe doped and (E)–(G) Cs-doped after 5 h sputtering followed by annealing. (A) and (E) are the STM topographic images of the stripe phase. (B) The corresponding dI/dV map. (C) and (F) The corresponding FTs of larger topographic images. (D) and (G) The line profiles along the ΓM directions in (C) and (F). The measurements were performed at V = −600 mV, I = 1000 pA for A and B, and V = −800 mV, I = 50 pA for (E).

Bi_2Se_3. The study of the temperature dependence of the stripe phase may also give additional insight in this context. We point out that at 25 K, i.e., the temperature at which the STS data were recorded, we did not realize the electronic superstructure.

V. CONCLUSIONS

In conclusion, the measurements presented in our study provide the first identification of coexisting TSS and electronic stripe ordering on the surface of TIs. We suggest that the stripe phase is a bulk state property. The periodic potential landscape whose periodicity is variable by choosing an appropriate dopant can open up great potentials for manipulating the electronic and thermoelectric properties of TIs. It is reasonable to anticipate that, similar to Fe and Cs atoms, a wide variety of other transition or alkali metals will enable specific tailoring of the electronic properties of TI's at RT. The electronic stripe ordering might be an avenue towards the future high temperature superconductivity in doped TI-based materials.[1–3]

ACKNOWLEDGMENTS

We are grateful to H. L. Meyerheim, A. Ernst and K. Zakeri Lori for valuable discussions. We acknowledge and appreciate C. Tusche for fruitful discussions and supporting this work with photoemission data. The Bi_2Se_3 crystals have been supplied by E. V. Chulkov.

[1]W. D. Wise, M. C. Boyer, K. Chatterjee, T. Kondo, T. Takeuchi, H. Ikuta, Y. Wang, and W. Hudson, Nat. Phys. **4**, 696–699 (2008).
[2]S. A. Kivelson, I. P. Bindloss, E. Fradkin, V. Oganesyan, J. M. Tranquada, A. Kapitulnik, and C. Howald, Rev. Mod. Phys. **75**, 1201–1241 (2003).
[3]K. C. Rahnejat, C. A. Howard, N. E. Shuttleworth, S. R. Schofield, K. Iwaya, C. F. Hirjibehedin, C. Renner, G. Aeppli, and M. Ellerby, Nat. Commun. **2**, 558 (2011).
[4]G. Grüner, Rev. Mod. Phys. **60**, 1129–1181 (1988).
[5]N. P. Ong and P. Monceau, Phys. Rev. B **16**, 3443–3455 (1977).
[6]R. V. Coleman, B. Giambattista, P. K. Hansma, A. Johnson, W. W. Mcnairy, and G. Slough, Adv. Phys. **37**, 559–644 (1988).
[7]A. Soumyanarayanan, M. M. Yee, Y. He, J. van Wezel, D. J. Rahn, K. Rossnagel, E. W. Hudson, M. R. Norman, and J. E. Hoffmann, Proc. Natl. Acad. Sci. U.S.A. **110**, 1623–1627 (2013).
[8]A. Fang, N. Ru, I. R. Fisher, and A. Kapitulnik, Phys. Rev. Lett. **99**, 046401 (2007).
[9]T.-H. Kim and W. Yeom, Phys. Rev. Lett. **109**, 246802 (2012).
[10]H. Morikawa, I. Matsuda, and S. Hasegawa, Phys. Rev. B **70**, 085412 (2004).
[11]S. Brazovskii, C. Brun, Z.-Z. Wang, and P. Monceau, Phys. Rev. Lett. **108**, 096801 (2012).
[12]K. J. Koski, C. D. Wessells, B. W. Reed, J. J. Cha, D. Kong, and Y. Cui, J. Am. Chem. Soc. **134**, 13773–13779 (2012).
[13]K. P. Chen, F. R. Chung, M. Wang, and K. J. Koski, J. Am. Chem. Soc. **137**, 5431–5437 (2015).
[14]J. Commons, APS March Meeting 2015, Abstract ID: BAPS.2015.NES.B5.4.
[15]Y. Okada, W. Zhou, D. Walkup, C. Dhital, S. D. Wilson, and V. Madhavan, Nat. Commun. **3**, 1158 (2012).
[16]H. Guo, "Can spontaneous symmetry breaking order develop in a topological phase?," preprint arXiv:1308.6343.
[17]L. Fu and C. L. Kane, Phys. Rev. B **76**, 045302 (2007).
[18]M. Z Hasan and C. L. Kane, Rev. Mod. Phys. **82**, 3045–3067 (2010).
[19]Y. Xia, D. Qian, D. Hsieh, L. Wray, A. Pal, H. Lin, A. Bansil, D. Grauer, Y. S. Hor, R. J. Cava, and M. Z. Hasan, Nat. Phys. **5**, 398–402 (2009).
[20]D. Hsieh, D. Qian, L. Wray, Y. Xia, Y. S. Hor, R. J. Cava, and M. Z. Hasan, Nature **452**, 970–974 (2008).
[21]H. M. Benia, C. Lin, K. Kern, and C. R. Ast, Phys. Rev. Lett. **107**, 177602 (2011).
[22]M. R. Scholz, J. Sánchez-Barriga, D. Marchenko, A. Varykhalov, A. Volykhov, L. V. Yashina, and O. Rader, Phys. Rev. Lett. **108**, 256810 (2012).
[23]T. Valla, Z.-H. Pan, D. Gardner, Y. S. Lee, and S. Chu, Phys. Rev. Lett. **108**, 117601 (2012).
[24]P. D. Pietro, M. Ortolani, O. Limaj, A. D. Gaspare, V. Giliberti, F. Giorgianni, M. Brahlek, N. Bansal, N. Koirala, S. Oh, P. Calvani, and S. Lupi, Nat. Nanotechnol. **8**, 556–560 (2013).
[25]C. H. Li, O. M. J. van't Erve, J. T. Robinson, Y. Liu, L. Li, and B. T. Jonker, Nat. Nanotechnol. **9**, 218–224 (2014).
[26]S. Roy, H. L. Meyerheim, K. Mohseni, A. Ernst, M. M. Otrokov, M. G. Vergniory, G. Mussler, J. Kampmeier, D. Grütmacher, C. Tusche, J. Schneider, E. V. Chulkov, and J. Kirschner, Phys. Rev. B **90**, 155456 (2014).
[27]S. Roy, H. L. Meyerheim, A. Ernst, K. Mohseni, C. Tusche, M. G. Vergniory, T. V. Menshchikova, M. M. Otroko, A. G. Ryabishchenkova,

Z. S. Aliev, M. B. Babanly, K. A. Kokh, O. E. Tereshchenko, E. V. Chulkov, J. Schneider, and J. Kirschner, Phys. Rev. Lett. **113**, 116802 (2014).
[28]R. Shokri, H. L. Meyerheim, S. Roy, K. Mohseni, A. Ernst, M. M. Otrokov, E. V. Chulkov, and J. Kirschner, Phys. Rev. B **91**, 205430 (2015).
[29]A. Cavallin, V. Sevriuk, K. N. Fischer, S. Manna, S. Ouazi, M. Ellguth, C. Tusche, H. L. Meyerheim, D. Sander, and J. Kirschner, Surf. Sci. **646**, 72–82 (2016).
[30]A. Polyakov, H. L. Meyerheim, E. D. Crozier, R. A. Gordon, K. Mohseni, S. Roy, A. Ernst, M. G. Vergniory, X. Zubizarreta, M. M. Otrokov, E. V. Chulkov, and J. Kirschner, Phys. Rev. B **92**, 045423 (2015).
[31]See the supplementary material at http://dx.doi.org/10.1063/1.4942220 for sample preparation including STM and AES data.
[32]T. Schlenk, M. Bianchi, M. Koleini, A. Eich, O. Pietzsch, T. O. Wehling, T. Frauenheim, A. Balatsky, J.-L. Mi, B. B. Iversen, J. Wiebe, A. A. Khajetoorians, P. Hofmann, and R. Wiesendanger, Phys. Rev. Lett. **110**, 126804 (2013).
[33]H. L. Meyerheim, S. Roy, K. Mohseni, A. Ernst, E. D. Crozier, R. Gordon, M. M. Otrokov, E. V. Chulkov, and J. Kirschner, "Understanding the electronic surface structure of cesium on Bi_2Se_3(0001)" (unpublished).
[34]B. Krömker, M. Escher, D. Funnemann, D. Hartung, H. Engelhard, and J. Kirschner, Rev. Sci. Instrum. **79**, 053702 (2008).
[35]H. Beidenkopf, P. Roushan, J. Seo, L. Gorman, I. Drozdov, Y. S. Hor, R. J. Cava, and A. Yazdani, Nat. Phys. **7**, 939–943 (2011).
[36]S. Kim, M. Ye, K. Kuroda, Y. Yamada, E. E. Krasovskii, E. V. Chulkov, K. Miyamoto, M. Nakatake, T. Okuda, Y. Ueda, K. Shimada, H. Namatame, M. Taniguchi, and A. Kimura, Phys. Rev. Lett. **107**, 056803 (2011).
[37]M. M. Yee, Z.-H. Zhu, A. Soumyanarayanan, Y. He, C. L. Song, E. Pomjakushina, Z. Salman, A. Kanigel, K. Segawa, Y. Ando, and J. E. Hoffman, Phys. Rev. B **91**, 161306(R) (2015).
[38]S. V. Eremeev, Y. M. Koroteev, and E. V. Chulkov, JETP Lett. **91**, 387–391 (2010).
[39]L. Fu, Phys. Rev. Lett. **103**, 266801 (2009).
[40]P. Roushan, J. Seo, C. V. Parker, Y. S. Hor, D. Hsieh, D. Qian, A. Richardella, M. Z. Hasan, R. J. Cava, and A. Yazdani, Nature **460**, 1106–1109 (2009).
[41]M. Bianchi, R. C. Hatch, Z. Li, P. Hofmann, F. Song, J. Mi, B. B. Iversen, Z. M. A. El-Fattah, P. Löptin, L. Zhou, A. A. Khajetoorian, J. Wiebe, R. Wiesendanger, and J. W. Wells, ACS Nano **6**, 7009–7015 (2012).
[42]M. Bianchi, D. Guan, S. Bao, J. Mi, B. B. Iversen, P. D. C. King, and P. Hofmann, Nat. Commun. **1**, 128 (2010).
[43]C. Domke, M. Heinrich, P. Elbert, and K. Urban, J. Vac. Sci. Technol., B **16**, 2825–2832 (1998).
[44]J. F. Zheng, X. Liu, N. Newman, E. R. Weber, D. F. Ogletree, and M. Salmeron, Phys. Rev. Lett. **72**, 1490 (1994).